Current Applied Physics 17 (2017) 1459–1464

Contents lists available at ScienceDirect

Current Applied Physics

journal homepage: www.elsevier.com/locate/cap

Comparative study for electrical transport characteristics of self-assembled monolayers formed by benzenethiol, cyclohexanethiol, and adamantanethiol

Junwoo Kim [a], Hyunhak Jeong [a], Sicheon Seong [b], Mingi Kim [c], Dongku Kim [a], Wang-Taek Hwang [a], Yeonsik Jang [a], Barbara Yuri Choi [a], Jeongmin Koo [a], Seung Bum Park [c], Jaegeun Noh [b, *], Takhee Lee [a, *]

[a] Department of Physics and Astronomy, Institute of Applied Physics, Seoul National University, Seoul 08826, South Korea
[b] Department of Chemistry and Institute of Nano Science and Technology, Hanyang University, Seoul 04763, South Korea
[c] CRI center for Chemical Proteomics, Department of Chemistry, Seoul National University, Seoul 08826, South Korea

ARTICLE INFO

Article history:
Received 17 June 2017
Received in revised form
8 August 2017
Accepted 16 August 2017
Available online 17 August 2017

Keywords:
Molecular electronics
Molecular device
Self-assembled monolayer
STM
Charge transport

ABSTRACT

We investigated the effect of molecular backbone structure on the electrical transport properties of self-assembled monolayer (SAM)-based molecular devices which were made with using three different molecules; benzenethiol (denoted as BT), cyclohexanethiol (CHT), and adamantanethiol (ADT). These molecules have similar ring-shaped backbone structures but different molecular orbital systems. The molecular devices were fabricated as a vertical metal-SAM-molecule structure by a conventional optical lithography-based microscale via-hole technique with employing PEDOT:PSS (poly(3,4-ethylenedioxythiophene)) stabilized with poly(4-styrenesulfonic acid) interlayer, which leads to a high device yield. We found that the current density of BT molecular devices was one order higher than that of CHT and ADT molecular devices due to the different molecular orbital systems. Also, we observed that the current densities of CHT and ADT devices were slightly different according to the statistical analysis because of the different structural uniformity of SAMs.

1. Introduction

The goal of molecular electronics as a future candidate for semiconductor-based electronics approaching its scalable limit is to utilize an individual or ensemble of molecules as an active material for electronic device components such as diode, transistor, switch, and sensor [1–10]. In order to pursue this aim, many research groups have performed in-depth studies on the fundamental charge transport characteristics of various molecules especially in the form of self-assembled monolayers (SAMs), which is an essential prerequisite for this purpose [11–20]. For example, there have been several studies focusing on the effect of backbone structures of the molecules on the charge transport characteristics using some accessible molecules: σ-saturated molecules (e.g. alkanethiols) [21], π-conjugated aromatic molecules (e.g. benzenethiols, or biphenylthiols) [22], and oligo(*p*-phenylene ethylene)s [23]. However, most of these studies have mainly been focused on the comparison between the molecules having completely different structural appearances, for example, π-conjugated oligoacene and σ-saturated alkanethiolate systems, in which their various intrinsic properties are obviously different [24]. On the other hand, this kind of comparison of the electrical characteristics with molecules that show similar molecular backbone structures but subtle differences in bonding properties may be helpful to gain a better understanding on the effect of backbone structures on the molecular charge transport mechanisms.

Here, we studied the structural and electrical properties of three different molecules: benzenethiol (denoted as BT) with a π-conjugated aromatic ring, cyclohexanethiol (CHT) with a σ-bonded flexible aliphatic ring, and adamantanethiol (ADT) with a σ-bonded rigid and spherical aliphatic ring. These molecules with the simple chemical structure can be the best model compounds for elucidating those issues compared with molecules containing a complicated structure. To this end, we fabricated a large number of

* Corresponding authors.
E-mail addresses: jgnoh@hanyang.ac.kr (J. Noh), tlee@snu.ac.kr (T. Lee).

http://dx.doi.org/10.1016/j.cap.2017.08.013
1567-1739/

ensemble molecular junctions as microscale via-hole structures using PEDOT:PSS (poly(3,4-ethylenedioxythiophene)) interlayer, which leads to the excellent device yield [25]. In particular, we examined how much the electrical transport properties are affected by the molecules containing π-conjugated aromatic ring and σ-bonded aliphatic ring as well as by the molecules containing two different σ-bonded aliphatic rings. We also examined whether the order and two-dimensional packing structure of SAMs with aliphatic cyclic ring (CHT and ADT) affected the electrical transport properties of SAM-based molecular electronic devices.

2. Experimental section

2.1. SAM preparation

The chemical structures of the molecules are shown in Fig. 1. BT, CHT, and ADT molecules were purchased (Tokyo Chemical Industry Co.) and used without further purification. The BT, CHT, and ADT SAMs were characterized using scanning tunneling microscopy (STM). For this, Au(111) substrates with atomically flat terraces in the range of 100–400 nm were prepared by thermally evaporating Au onto a fleshly cleaved mica plate, as previously described [26]. Then, BT, CHT, and ADT SAMs were prepared by immersing the Au(111) substrates in a 1 mM ethanol solution of the corresponding molecules at room temperature for 24 h in a N_2-filled glove box. After SAM-deposited Au samples were taken from the solutions, they were thoroughly rinsed with pure ethanol to remove weakly adsorbed molecules. STM measurements were carried out under ambient conditions using a NanoScope E with a commercially available Pt/Ir tip (80:20). All STM images were obtained using the constant current mode. During the STM imaging, bias voltage ranging from 300 to 550 mV and tunneling current ranging from 200 to 500 pA were applied.

2.2. Electrical transport measurement

To characterize the electronic transport properties of BT, CHT, and ADT SAMs, we fabricated molecular devices employing a poly (3,4-ethylenedioxythiophene) polystyrene sulfonate (called as PEDOT:PSS) as an interlayer between the SAMs and top metal electrodes in the vertical M-SAM-M structure. Fig. 2 shows the schematic illustrations of device fabrication processes. We followed the similar fabrication process that has been widely used by several groups [27–30]. Briefly, the bottom electrodes (50 nm Au/5 nm Ti) were first deposited on a p++ SiO_2/Si substrate by an electron beam evaporator at a deposition rate of 0.2 Å/s. Patterned shadow mask was used for bottom electrode patterning. Then, photoresist (AZ 5214E) was spin-coated and conventional photolithography process was performed. Bottom electrodes are squares with a side length of 20 or 40 μm. Then, SAMs were formed on the bottom electrodes by immersing the samples in 1 mM ethanol solutions of the corresponding molecules for 24 h at room temperature in a N_2-filled glove box. The samples were rinsed by using pure ethanol to eliminate physisorbed molecules on SAMs. The rinsed samples were dried for ~3 h in a vacuum desiccator. PEDOT:PSS (Clevios PH 1000) was spin-coated on the substrate and dried for ~3 h in the vacuum desiccator. As an interlayer, PEDOT:PSS prevents devices from the formation of filamentary conducting path during top electrode deposition. After the PEDOT:PSS deposition, we deposited Au top electrode (30 nm thick) using the electron beam evaporator at a deposition rate of 0.2 Å/s via patterned shadow masks. Finally, residual PEDOT:PSS was removed with a reactive ion etcher using O_2 gas (50 sccm, 100 W). Fig. 2(b) shows the optical, scanning electron microscopy (SEM), and cross-sectional transmission electron microscopy (TEM) images of fabricated molecular devices. Particularly, from the TEM image, we observed that penetration of gold through PEDOT:PSS interlayer had not occurred. The fabricated molecular devices were characterized using a semiconductor parameter analyzer (Model 4200 SCS, Keithley) for the electrical characterizations.

3. Results and discussion

Fig. 3 shows the high-resolution STM images of BT, CHT, and ADT SAMs formed on Au substrates. BT SAMs with a π-conjugated aromatic ring were mainly composed of the disordered phase with SAM-covered Au adatom islands (bright islands), as shown in Fig. 3(a). The formation mechanism of these Au adatom islands has been discussed in our review paper [31]. Many STM studies also showed the similar surface structure, so that the Au adatom islands can be considered as the intrinsic surface characteristics for BT SAMs. In contrast to BT SAMs, CHT and ADT SAMs with σ-bonded aliphatic cyclic rings had long-range ordered phases, as shown in Fig. 3(b) and (c). Molecular-scale STM imaging clearly revealed that CHT SAMs on Au(111) in the inset of Fig. 3(b) have a zig-zag bright and dark molecular row structure, which has also been visualized in our previous works [32–34] and others [35]. This unique packing structure is attributed to the existence of two energetically stable conformers, i.e., equatorial and axial conformers resulting from a conformation change of 6-membered aliphatic cyclic ring [32]. The packing structure for CHT SAMs is assigned as a $(5 \times 2\sqrt{3})R35^\circ$ superlattice and the average areal density for the CHT SAMs was calculated to be 36.09 $Å^2$/molecule. The structural details were discussed in earlier papers [34]. CHT SAMs had a corrugated packing structure, whereas ADT SAMs with a bulky, spherical aliphatic ring backbone have a very uniform and hexagonal close-

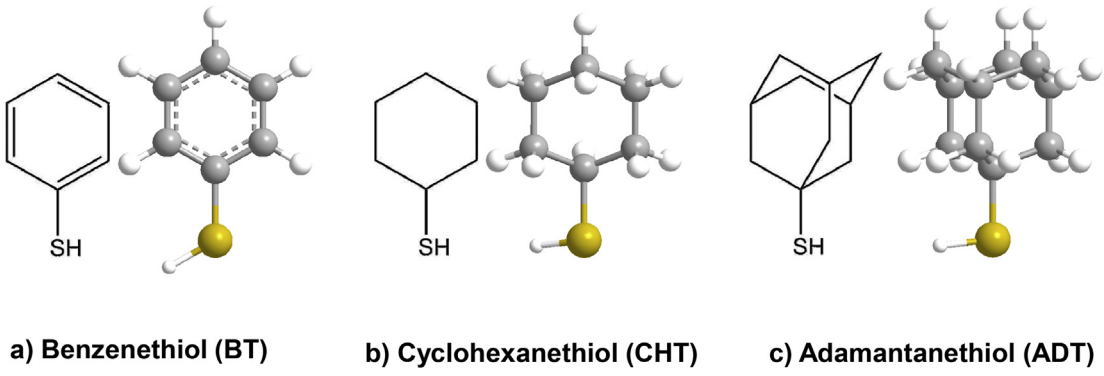

Fig. 1. Chemical structures of three molecules used in this study: (a) BT, (b) CHT, and (c) ADT.

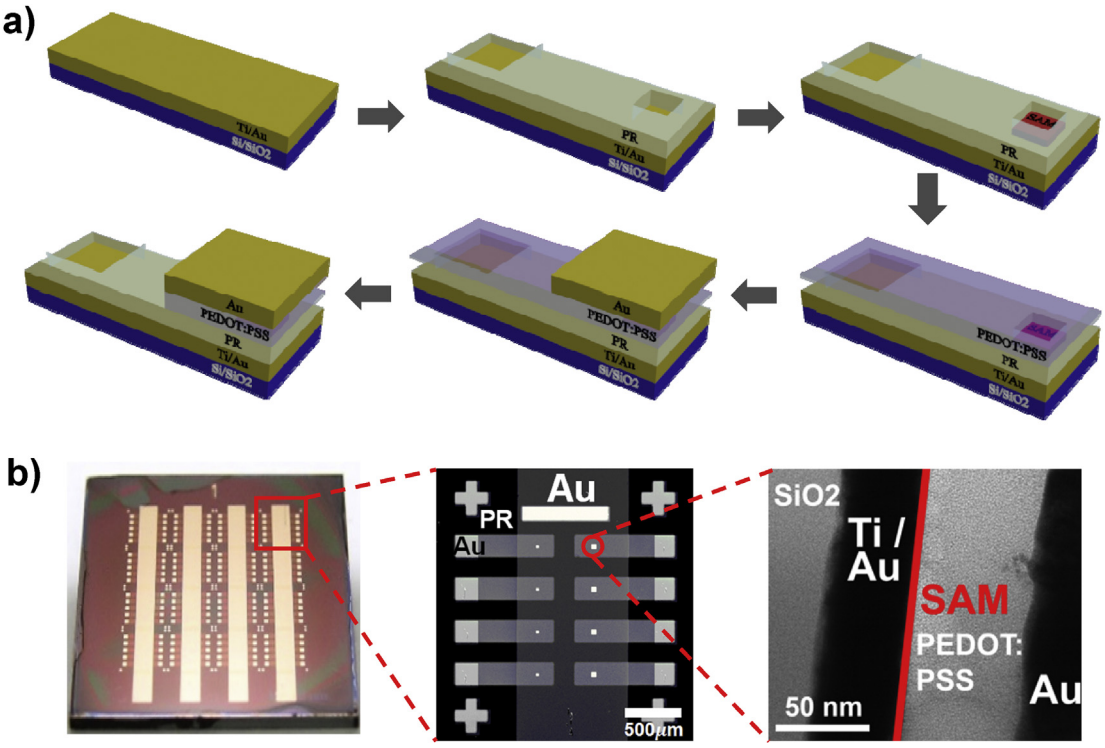

Fig. 2. (a) Schematic illustration of molecular device fabrication process. (b) Optical, SEM, and TEM images of fabricated molecular devices.

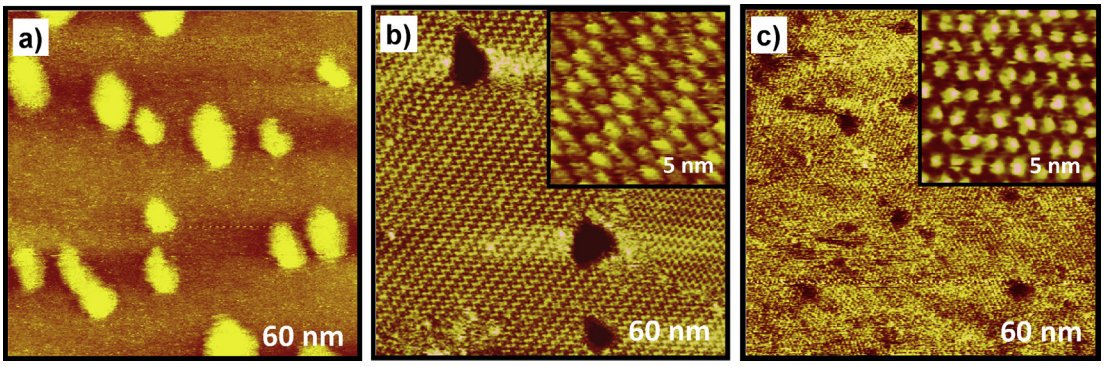

Fig. 3. STM images of (a) BT, (b) CHT, and (c) ADT SAMs on Au(111) showing the structural differences. The scan sizes of all STM images were 60 nm × 60 nm. The 5 nm × 5 nm inset STM images in (b) and (c) show a high degree of the structural order for CHT and ADT SAMs on Au(111).

packed structure with a nearest neighbor distance of 6.9 ± 0.3 Å and a next nearest neighbor distance of 11.8 ± 0.3 Å, as shown in the inset of Fig. 3(c). This packing structure for ADT SAMs is nearly similar to that revealed by Dameron et al. [36], which can be assigned as a (7 × 7) structure and the average areal density was calculated to be 47.61 $Å^2$/molecule. We also found that the ordered domains for CHT SAMs contained relatively large vacancy islands (dark holes) with a size of 5–15 nm, whereas ADT SAMs had a number of small vacancy islands with a size of 2–5 nm. In addition, domain boundaries were clearly observed for CHT SAMs, but no clear domain boundaries were observed for ADT SAMs. From our STM study, we directly compared the surface structures of BT, CHT, and ADT SAMs on Au(111) and revealed the large differences in the domain formation and surface structure of SAMs depending on the chemical structure of molecular backbone.

Then, we studied the electronic transport characteristics of the molecular devices that were made with the BT, CHT, and ADT SAMs. Fig. 4(a) shows the mean current density versus voltage (J-V) characteristics of BT, CHT, and ADT molecular devices. In addition, we plotted a two-dimensional color map of the logarithmic current density versus voltage of all 384 measured devices of BT, CHT, and ADT molecules, as shown in Fig. 4(b). The current densities of CHT and ADT molecular devices appeared similar, whereas that of BT molecular devices was higher by approximately an order of magnitude than those of CHT and ADT molecular devices. This difference of current densities among the different molecular species is attributed to their different electronic orbital structures among them; several i.e., BT has a π-conjugated system, whereas CHT and ADT have σ-saturated system, thus the electrical transport property of BT is more efficient than CHT and ADT due to the delocalized π-electrons of phenyl ring of BT [25]. In the cases of CHT and ADT, these two molecules are all σ-bonded system and have similar molecular length (Fig. 1), which results in similar current level. Also, we measured the J-V characteristics of several tens of

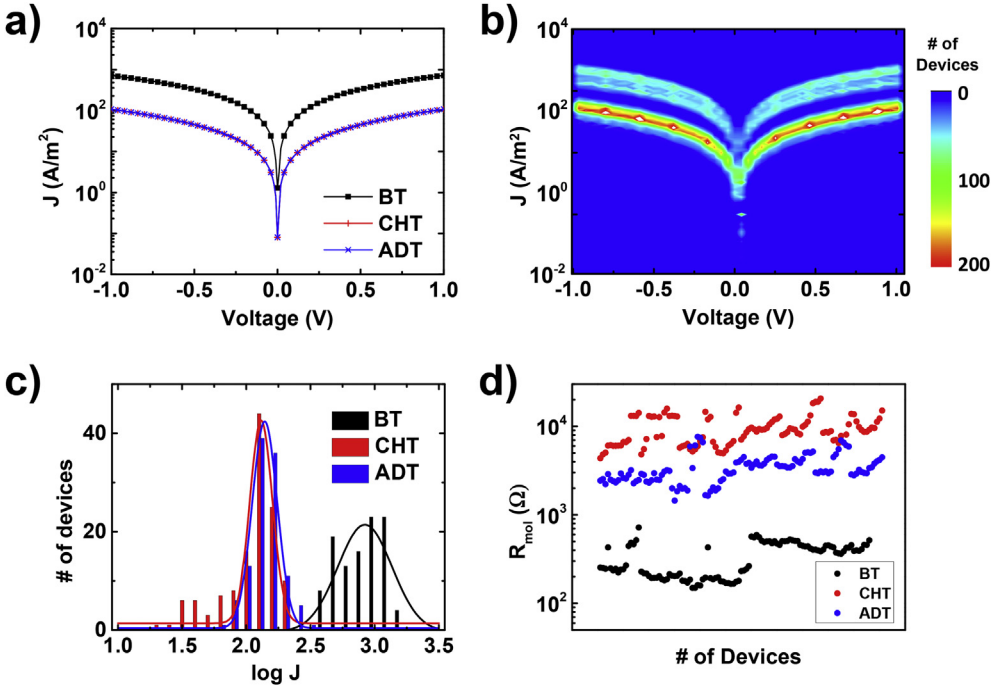

Fig. 4. (a) Mean J-V characteristic of all BT, CHT, and ADT working molecular devices. (b) Two-dimensional semi-logarithmic J-V histogram plot for all working molecular devices. (c) Histogram of log J at 1 V for all molecular devices including non-working ones. (d) The resistance per molecule R_{mol} for BT, CHT, ADT molecular junctions.

devices without SAMs between the electrodes as a control group. From the results, it is found that their J values were approximately 10^4 A/m^2 at 1 V voltage (data are not shown here), which demonstrates that the electrical characteristics of devices with SAMs were mainly determined by the molecular species. The currents passing via gold only were above 0.1 A at 1 V, which exceeded the compliance of all measurement. Therefore, we can say that current characteristics of the control group represents metal-air-PEDOT:PSS-metal transport, not via gold penetration. Based on the discussion above, the charge conduction mainly occurs through metal-SAMs-PEDOT:PSS-metal rather than metal-air-PEDOT:PSS-metal.

Fig. 4(c) displays the histogram of logarithmic current densities for all the measured molecular devices except the electrically short devices. We observed that there were no fabrication failures or electrically open devices. Table 1 summarized the detailed statistical analysis results for BT, CHT, and ADT molecular devices in this study. Among the fabricated 384 molecular devices, 328 devices were found to be presumably "working" molecular devices. We used our previous statistical criteria for selecting 'working' devices [37]. To briefly explain, we made a histogram of logarithmic current densities (at 1 V) of all the measured molecular devices, then fitted the histogram to a Gaussian distribution using least squares method. The range of working device was determined from $\mu - 3\sigma$ to $\mu + 3\sigma$, where μ and σ are the Gaussian average and standard deviation of the current densities, respectively. Following this principle, the device yield was determined to be 85.4%. This device yield is close to the yield values (~90%) previously reported for the molecular devices made by similar fabrication method [6,27,28,30]. Our results with PEDOT:PSS buffer layer far outweigh the device yield using top electrode deposition without interlayer, which turned out less than 1%, demonstrating that PEDOT:PSS effectively functioned as a buffer layer, preventing molecular devices from gold penetration [38]. The mean logarithmic current density at 1 V of BT molecular devices was 2.92 (corresponding to J ~ 840 A/m^2), which is higher than that of CHT (2.11, corresponding to J ~ 131 A/m^2) and ADT (2.14 corresponding to J ~ 139 A/m^2).

Furthermore, we have performed DFT calculation of BT, CHT and ADT. The calculations were performed using Gaussian09W program at the B3LYP6-31G level. The results showed that HOMO-LUMO gap of BT (6.08 eV) was smaller than those of other molecules; CHT (7.04 eV) and ADT (6.92 eV) showed relatively similar HOMO-LUMO gaps. As far as we know, the HOMO-LUMO gaps of CHT and ADT have not been reported. But for BT, its HOMO-LUMO gap has been reported as 4.09 eV, which is somewhat different from our calculated data [39]. This is due to the fact that we assumed one isolated gas molecule system to estimate the HOMO-LUMO gaps. These results demonstrate that the difference of electronic structure due to molecular backbone variation significantly influences the electrical transport characteristics.

Meanwhile, SAM structural properties can also affect the electrical transport characteristics of molecular devices, especially on the statistical perspective. Each molecule has differing standard deviation of the logarithmic current densities when the molecules

Table 1
Summary of the statistical analysis results for all fabricated molecular devices.

Molecules	Number of fabricated devices	Fab. failure	Short	Open	Non-working	Working	Device yield
BT	128 (100.0%)	0 (0.0%)	22 (7.0%)	0 (0.0%)	0 (0.0%)	106 (82.8%)	
CHT	128 (100.0%)	0 (0.0%)	1 (0.8%)	0 (0.0%)	16 (12.5%)	111 (86.7%)	328 (85.4%)
AT	128 (100.0%)	0 (0.0%)	17 (13.3%)	0 (0.0%)	0 (0.0%)	111 (86.7%)	

are formed as SAM. This phenomenon comes from the different SAM structure due to distinct molecular structural property. Conformational SAM structure, such as packing density or ordering, could be the factor that influences the electrical transport property through the molecular junction. Several studies revealed that BT SAM contains mainly disordered phases including many Au adatom islands [33]. In addition, CHT and ADT SAMs have more ordered structures compared to BT SAMs, as revealed by STM study (Fig. 3). Therefore, the distribution in the histogram of BT molecular devices was the most disordered among the three molecules (Fig. 4(c)). On the other hand, the standard deviation of CHT logarithmic current density distribution (0.0879) was ~10% larger than that of ADT (0.0976), and more non-working devices was found for CHT (16 devices) than ADT (0 device). We assumed that these results are probably due to the difference in structural quality of two ordered SAMs, as demonstrated by STM study (Fig. 3). CHT molecules with a flexible aliphatic ring have ordered SAMs containing two equatorial and axial conformers (different adsorption geometry) and clear domain boundaries (Fig. 3(b)), whereas ADT molecules with relatively more rigid body have more uniform SAMs with single molecular feature and no domain boundaries (Fig. 3(c)). However, the differences in standard deviation and the number of non-working devices between CHT- and ADT-based devices are not so significant, therefore we can tell that in case of σ-saturated system, the rigidity of molecular backbone hardly influences the electrical transport characteristics.

Fig. 4(d) shows a plot of the resistance per mol (Rmol) for all the measured BT, CHT, and ADT molecular devices (328 devices). The resistance values were determined by linear fittings at low bias (from −0.01 to 0.01 V) from J-V data curves, and Rmol values were calculated by assuming 7.09 μmol/m^2 for BT [18], 1.89 μmol/m^2 for CHT [34], and 4.22 μmol/m^2 for ADT [36]. This plot clearly shows that the resistance of BT devices is lower than that of CHT and ADT devices, nearly by an order of magnitude due to aforementioned reasons. Note that the contact properties between PEDOT:PSS and molecules cannot be a reason for different resistances among BT, CHT and ADT devices, because all the three types of molecular devices commonly had methyl-based terminal group.

4. Conclusions

In summary, we investigated the topography of the SAMs on Au surface and their effects on the electrical transport characteristics of BT, CHT, and ADT molecules that have cyclic ring structures. The surface of BT SAM showed disordered phases with Au adatom islands, while those of CHT and ADT SAMs presented long-range ordered phases. In addition, ADT SAMs had more uniform structure with no clear domain boundaries than CHT SAMs. From the perspective of the charge transport characteristics, the current densities through Au-BT SAM-PEDOT:PSS-Au junctions were nearly an order of magnitude higher than those of CHT and ADT molecular junctions, due to delocalized π-electrons of BT. Furthermore, similar current densities were observed between the CHT and ADT molecular junctions, in spite of different structural quality of SAMs, which indicates the rigidity of σ-saturated molecular backbone has insignificant influence on the electrical transport characteristics. This study may be beneficial to understand better the effect of backbone structures on the molecular charge transport characteristics.

Acknowledgments

This work was supported by National Creative Research Laboratory Program (grant no. 2012026372) provided by the National Research Foundation of Korea (NRF), funded by the Korean Ministry of Science and ICT and Basic Science Research Program through the National Research Foundation of Korea (NRF) funded by the Ministry of Education (NRF-2012R1A6A1029029 & NRF-2015R1D1A1A01058769).

References

[1] A. Aviram, M.A. Ratner, Molecular rectifiers, Chem. Phys. Lett. 29 (1974) 277–283.
[2] A. Nitzan, M.A. Ratner, Electron transport in molecular wire junctions, Science 300 (2003) 1384–1389.
[3] D. Xiang, X. Wang, C. Jia, T. Lee, X. Guo, Molecular-scale electronics: from concept to function, Chem. Rev. 116 (2016) 4318–4440.
[4] J.C. Cuevas, E. Scheer, Molecular Electronics: an Introduction to Theory and Experiment, World Scientific Publishing, Singapore, 2010.
[5] H. Song, Y. Kim, Y.H. Jang, H. Jeong, M.A. Reed, T. Lee, Observation of molecular orbital gating, Nature 462 (2009) 1039–1043.
[6] D. Kim, H. Jeong, H. Lee, W.T. Hwang, J. Wolf, E. Scheer, T. Huhn, H. Jeong, T. Lee, Flexible molecular-scale electronic devices composed of diarylethene photoswitching molecules, Adv. Mater. 26 (2014) 3968–3973.
[7] N. Nerngchamnong, L. Yuan, D.C. Qi, J. Li, D. Thompson, C.A. Nijhuis, The role of van der Waals forces in the performance of molecular diodes, Nat. Nanotechnol. 8 (2013) 113–118.
[8] M.L. Perrin, E. Galan, R. Eelkema, J.M. Thijssen, F. Grozema, H.S.J. van der Zant, A gate-tunable single-molecule diode, Nanoscale 8 (2016) 8919–8923.
[9] H.J. Yoon, K.C. Liao, M.R. Lockett, S.W. Kwok, M. Baghbanzadeh, G.M. Whitesides, Rectification in tunneling junctions: 2,2′-bipyridyl-terminated n-alkanethiolates, J. Am. Chem. Soc. 136 (2014) 17155–17162.
[10] B. Capozzi, J.L. Xia, O. Adak, E.J. Dell, Z.F. Liu, J.C. Taylor, J.B. Neaton, L.M. Campos, L. Venkataraman, Single-molecule diodes with high rectification ratios through environmental control, Nat. Nanotechnol. 10 (2015) 522–527.
[11] M.A. Karimi, S.G. Bahoosh, M. Herz, R. Hayakawa, F. Pauly, E. Scheer, Shot noise of 1,4-benzenedithiol single-molecule junctions, Nano Lett. 16 (2016) 1803–1807.
[12] J. Sporrer, J.H. Chen, Z.J. Wang, M.M. Thuo, Revealing the nature of molecule-electrode contact in tunneling junctions using raw data heat maps, J. Phys. Chem. Lett. 6 (2015) 4952–4958.
[13] H. Lissau, R. Frisenda, S.T. Olsen, M. Jevric, C.R. Parker, A. Kadziola, T. Hansen, H.S.J. van der Zant, M.B. Nielsen, K.V. Mikkelsen, Tracking molecular resonance forms of donor-acceptor push-pull molecules by single-molecule conductance experiments, Nat. Commun. 6 (2015).
[14] Y. Majima, D. Ogawa, M. Iwamoto, Y. Azuma, E. Tsurumaki, A. Osuka, Negative differential resistance by molecular resonant tunneling between neutral tribenzosubporphine anchored to a Au(111) surface and tribenzosubporphine cation adsorbed on to a tungsten tip, J. Am. Chem. Soc. 135 (2013) 14159–14166.
[15] G.D. Kong, M. Kim, S.J. Cho, H.J. Yoon, Gradients of rectification: tuning molecular electronic devices by the controlled use of different-sized diluents in heterogeneous self-assembled monolayers, Angew. Chem. Int. Ed. 55 (2016) 10307–10311.
[16] T. Kim, P. Darancet, J.R. Widawsky, M. Kotiuga, S.Y. Quek, J.B. Neaton, L. Venkataraman, Determination of energy level alignment and coupling strength in 4,4′-bipyridine single-molecule junctions, Nano Lett. 14 (2014) 794–798.
[17] S. Seo, M. Min, J. Lee, T. Lee, S.Y. Choi, H. Lee, Solution-processed reduced graphene oxide films as electronic contacts for molecular monolayer junctions, Angew. Chem. Int. Ed. 51 (2012) 108–112.
[18] L.J. Wan, M. Terashima, H. Noda, M. Osawa, Molecular orientation and ordered structure of benzenethiol adsorbed on gold (111), J. Phys. Chem. B 104 (2000) 3563–3569.
[19] D. Thompson, C.A. Nijhuis, Even the odd numbers help: failure modes of SAM-based tunnel junctions probed via odd-even effects revealed in synchrotrons and supercomputers, Acc. Chem. Res. 49 (2016) 2061–2069.
[20] T.W. Lee, J.W.P. Hsu, Molecular monolayer modification of the cathode in organic light-emitting diodes, Appl. Phys. Lett. 89 (2006) 223511.
[21] J.M. Beebe, B. Kim, J.W. Gadzuk, C.D. Frisbie, J.G. Kushmerick, Transition from direct tunneling to field emission in metal-molecule-metal junctions, Phys. Rev. Lett. 97 (2006).
[22] Y. Jang, H. Jeong, D. Kim, W.-T. Hwang, J.W. Kim, I. Jeong, H. Song, J. Yoon, G.C. Yi, H. Jeong, T. Lee, Electrical characterization of benzenedithiolate molecular electronic devices with graphene electrodes on rigid and flexible substrates, Nanotechnology 27 (2016) 145301.
[23] Q. Lu, K. Liu, H.M. Zhang, Z.B. Du, X.H. Wang, F.S. Wang, From tunneling to hopping: a comprehensive investigation of charge transport mechanism in molecular junctions based on oligo(p-phenylene ethynylene)s, ACS Nano 3 (2009) 3861–3868.
[24] G. Wang, T.W. Kim, Y.H. Jang, T. Lee, Effects of metal-molecule contact and molecular structure on molecular electronic conduction in nonresonant tunneling regime: alkyl versus conjugated molecules, J. Phys. Chem. C 112 (2008) 13010–13016.
[25] G. Wang, T.W. Kim, T. Lee, Electrical transport characteristics through molecular layers, J. Mater. Chem. 21 (2011) 18117–18136.
[26] S.Y. Lee, E. Ito, H. Kang, M. Hara, H. Lee, J. Noh, Surface structure, adsorption,

and thermal desorption behaviors of methaneselenolate monolayers on Au(111) from dimethyl diselenides, J. Phys. Chem. C 118 (2014) 8322–8330.
[27] H.B. Akkerman, P.W. Blom, D.M. De Leeuw, B. De Boer, Towards molecular electronics with large-area molecular junctions, Nature 441 (2006) 69–72.
[28] H. Jeong, D. Kim, G. Wang, S. Park, H. Lee, K. Cho, W.T. Hwang, M.H. Yoon, Y.H. Jang, H. Song, D. Xiang, T. Lee, Redox-induced asymmetric electrical characteristics of ferrocene-alkanethiolate molecular devices on rigid and flexible substrates, Adv. Funct. Mater. 24 (2014) 2472–2480.
[29] S. Park, G. Wang, B. Cho, Y. Kim, S. Song, Y. Ji, M.H. Yoon, T. Lee, Flexible molecular-scale electronic devices, Nat. Nanotechnol. 7 (2012) 438–442.
[30] G. Wang, S.I. Na, T.W. Kim, Y. Kim, S. Park, T. Lee, Effect of PEDOT: PSS–molecule interface on the charge transport characteristics of the large-area molecular electronic junctions, Org. Electron. 13 (2012) 771–777.
[31] G.H. Yang, G.Y. Liu, New insights for self-assembled monolayers of organothiols on Au(111) revealed by scanning tunneling microscopy, J. Phys. Chem. B 107 (2003) 8746–8759.
[32] S.W. Joo, H. Chung, K. Kim, J. Noh, Conformational changes of cyclohexanethiol adsorbed on gold surfaces, Surf. Sci. 601 (2007) 3196–3201.
[33] H. Kang, H. Lee, Y. Kang, M. Hara, J. Noh, Two-dimensional ordering of benzenethiol self-assembled monolayers guided by displacement of cyclohexanethiols on Au(111), Chem. Commun. (2008) 5197–5199.
[34] S. Kwon, Y. Jeong, Y. Lee, J. Noh, A new superlattice of cyclohexanethiol self-assembled monolayers on Au (111) formed at a low solution temperature, Chem. Lett. 36 (2007) 390–391.
[35] P.S. Luo, N.L. Bemelmans, T.P. Pearl, Unveiling molecular adsorption geometry in cyclohexanethiolate self-assembled monolayers with local barrier height imaging, J. Phys. Chem. C 115 (2011) 17118–17122.
[36] A.A. Dameron, L.F. Charles, P.S. Weiss, Structures and displacement of 1-adamantanethiol self-assembled monolayers on Au{111}, J. Am. Chem. Soc. 127 (2005) 8697–8704.
[37] H. Jeong, D. Kim, H. Kwon, W.-T. Hwang, Y. Jang, M. Min, K. Char, D. Xiang, H. Jeong, T. Lee, Statistical investigation of the length-dependent deviations in the electrical characteristics of molecular electronic junctions fabricated using the direct metal transfer method, J. Phys. Condens. Matter 28 (2016) 094003.
[38] T.W. Kim, G. Wang, H. Lee, T. Lee, Statistical analysis of electronic properties of alkanethiols in metal–molecule–metal junctions, Nanotechnology 18 (2007) 315204.
[39] M.R. Gartia, T.C. Bond, G.L. Liu, Metal-Molecule Schottky junction effects in surface enhanced Raman scattering, J. Phys. Chem. A 115 (2011) 318–328.